Journal of Materials Chemistry C

PAPER

View Article Online
View Journal | View Issue

Cite this: J. Mater. Chem. C, 2014, 2, 8350

Electrochemically created highly surface roughened Ag nanoplate arrays for SERS biosensing applications†

Shikuan Yang,*[a] Daniel Slotcavage,[a] John D. Mai,[b] Feng Guo,[a] Sixing Li,[ac] Yanhui Zhao,[a] Yong Lei,[d] Craig E. Cameron[c] and Tony Jun Huang*[a]

Received 15th June 2014
Accepted 27th August 2014

DOI: 10.1039/c4tc01276c

www.rsc.org/MaterialsC

Highly surface-roughened Ag nanoplate arrays are fabricated using a simple electrodeposition and *in situ* electrocorrosion method with inorganic borate ions as capping agent. The electrocorrosion process is induced by a change in the local pH value during the electrochemical growth, which is used to intentionally carve the electrodeposited structures. The three dimensionally arranged Ag nanoplates are integrated with substantial surface-enhanced Raman scattering (SERS) hot spots and are free of organic contaminations widely used as shaping agents in previous works, making them excellent candidate substrates for SERS biosensing applications. The SERS enhancement factor of the rough Ag nanoplates is estimated to be $>10^9$. These Ag nanoplate arrays are used for SERS-based analysis of DNA hybridization monitoring, protein detection, and virus differentiation without any additional surface modifications or labelling. They all exhibit an extremely high detection sensitivity, reliability, and reproducibility.

1. Introduction

Surface-enhanced Raman scattering (SERS) is considered to be one of the most promising techniques for biosensing.[1] SERS provides vibrational spectra information that enables rapid, label-free, highly specific, and extremely sensitive detection.[1–5] While multiple mechanisms contribute to the exceptional sensitivity of SERS, it is widely accepted that electromagnetic effects account for the majority of its significant improvement over traditional Raman scattering.[6–8] This electromagnetic enhancement often occurs in the vicinity of noble metal nanostructures exhibiting plasmonic resonances and is largest at the hot spots near the rough sites (<10 nm) where electromagnetic fields are highly localized.[9–12] A high density of hot spots generally corresponds to improved SERS sensitivity and is essential for SERS-based sensing.[13–21]

Nanoplate structures are generally considered as one of the most promising SERS substrates and they have been shown to have a higher SERS enhancement effect than many other SERS structures such as nanocubes and nanospheres.[21,22] This is because of the significantly enhanced electromagnetic field around the corners and sharp edges of nanoplates.[22] There have already been many studies focused on the preparation of smooth nanoplate structures.[23,24] However, to further enhance the SERS sensitivity, highly surface roughened nanoplates are highly required. On the other hand, the anisotropic structure of nanoplates means that organic capping agents (for example, polyvinylpyrrolidone with a molecular weight of at least several kDa) are generally required in their synthesis.[23,24] Once introduced, these organic capping agents are difficult to remove completely (although plasma cleaning can partially remove the organic agents from nanostructures, the desirable features of the nanostructures may be simultaneously damaged), introducing surface-contaminants, and severely hindering the diffusion of analyte molecules into the hot spots.[25] Furthermore, post-synthesis assembly is required to fabricate immobilized substrates as dealing with the free-standing nanoplates prepared by wet chemical methods,[26] which is unfavorable in many applications. Electrochemical deposition has been developed to prepare nanostructures directly on a substrate usually at the assistance of specific surfactants,[27–29] whereas the structure of the electrodeposited materials, particularly the roughness, is often hard to control. Therefore, a method that enables the direct fabrication of highly surface roughened nanoplate substrates without the use of organic capping agents is highly desirable for SERS applications.

Here, we demonstrate a single-step electroplating/corrosion method for preparing large-area, highly surface roughened Ag

[a]Department of Engineering Science and Mechanics, The Pennsylvania State University, University Park, PA 16802-6812, USA. E-mail: szy2@psu.edu; junhuang@psu.edu

[b]Department of Mechanical and Biomedical Engineering, City University of Hong Kong, Tat Chee Avenue, Kowloon, Hong Kong SAR, China

[c]Department of Biochemistry and Molecular Biology, The Pennsylvania State University, University Park, PA 16802, USA

[d]Center for Innovation Competence & Institute for Physics, Technical University of Ilmenau, 98693 Ilmenau, Germany

† Electronic supplementary information (ESI) available: Experimental details, calculation of SERS enhancement factors, SEM images, FDTD simulation results, and UV-Vis absorption spectrum. See DOI: 10.1039/c4tc01276c

nanoplate arrays on a substrate without the use of any organic capping agent. Most importantly, an electrocorrosion process caused by a local change in pH value during electrochemical growth is utilized for the first time to carve the electrodeposited nanostructures, giving rise to the formation of highly surface-roughened Ag nanoplates. The roughened Ag nanoplates are excellent SERS substrates with a high hot-spot density ($>10^3$ per μm^2, see note ref. 30). To date, this is among the highest hot-spot densities achieved using nanoplates. The enhancement factor for SERS applications is estimated to be $>10^9$. The increased sensitivity combined with a simple, low-cost fabrication process make these Ag nanoplates excellent candidates for SERS-based biosensing, medical diagnostics, and energy harvesting applications.[31] As a proof-of-concept, we employed the as-prepared Ag nanoplate array to detect DNA, proteins, and viruses without additional surface functionalization. All of these biodetection experiments exhibit excellent specificity and reproducibility. For example, the substrates produced distinct SERS spectra even when examining small mutations in strains of specific viruses.

2. Results and discussion

2.1 Fabrication of Ag nanoplates with a high surface roughness

Electrochemical deposition/corrosion was used to create the roughened surfaces of the Ag nanoplate arrays (inset in Fig. 1a). Unlike those traditional methods[23–29] that employ organic chemicals, we used BO_3^{3-} ions as shaping agents. This effectively avoided organic contamination and better facilitated subsequent SERS sensing applications. The electrolyte solution

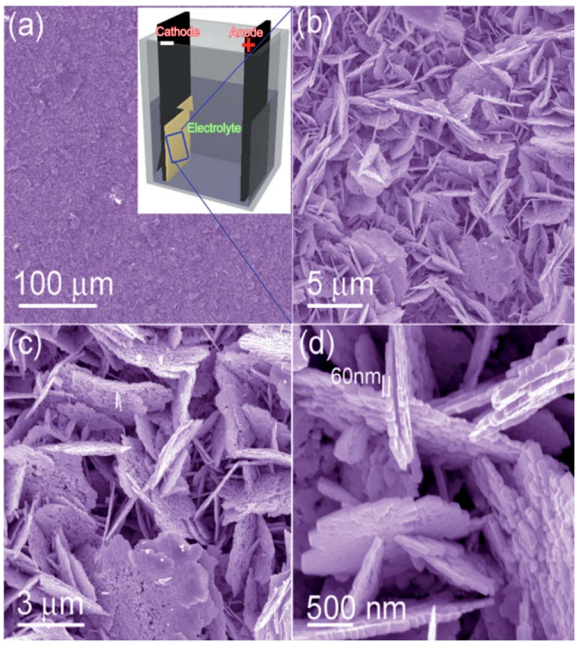

Fig. 1 (a–d) SEM images of the highly surface-roughened Ag nanoplate array at different magnifications. Inset in (a): schematic illustration of the electrochemical deposition cell.

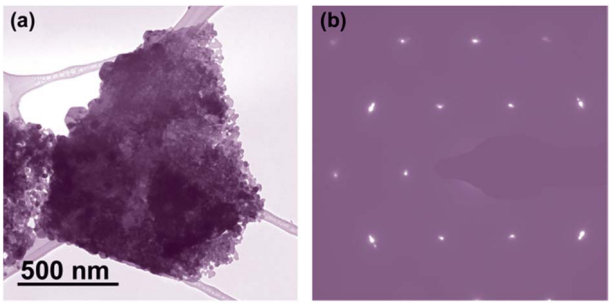

Fig. 2 (a) TEM image of the highly surface-roughened Ag nanoplates. (b) Selected area electron diffraction pattern.

was prepared by dissolving an equal amount (10 g) of $AgNO_3$ and H_3BO_3 (boric acid) into 1 L of deionized (DI) water. Electrochemical deposition was carried out in a double-electrode system under a potentiostatic mode. Two pieces of boron-doped silicon wafers (resistivity: 0.2 Ω cm) were used as anode and cathode with a working area of about 1 cm^2. The voltage applied between the two electrodes was 10 V.

Fig. 1 presents scanning electron microscope (SEM) images of the deposited Ag nanostructures. At low magnifications, a uniform morphology (see note ref. 32) is observed across the electrode surface (Fig. 1a). Enlarged images revealed more details of the individual nanoplates. Fig. 1b shows that nanoplates tended to cross-link together and have a slanted orientation relative to the substrate. Fig. 1c and d highlight the thinness of these Ag nanoplates (~60 nm) and clearly show their rough edges. Additionally, Fig. 1c and d demonstrate that the nanoplates possess a significant number of pits and steps on their surfaces, endowing them with many hot spots and making them ideal candidates as excellent SERS substrates. Transmission electron microscope (TEM) measurement was conducted on the highly surface-roughened Ag nanoplates released from the substrate by a supersonic treatment in ethanol (Fig. 2a). The selected area electron diffraction pattern (Fig. 2b) proves that the Ag nanoplates are single crystalline, which is in accordance with the electro-etching formation mechanism of the coarse Ag nanoplates proposed below.

2.2 Growth process of the Ag nanoplates

In order to investigate the growth process of these Ag nanoplates, we observed the resulting morphologies of the products prepared at different deposition times ranging from 10 s to 10 h (ESI, Fig. S1 and S2†). Based on the analysis of the experimental results (details can be found in the ESI†), we proposed a mechanism for the rough Ag nanoplate formation process (Fig. 3). Briefly, at the onset of deposition, Ag nuclei grow into small nanoplates due to the preferential adsorption of borate ions (BO_3^{3-}) on the Ag {111} planes. This severely inhibits Ag growth along the {111} planes, forcing the growth of anisotropically structured nanoplates. This shaping process is evidenced by the coexistence of spherical Ag nanoparticles and small Ag nanoplates at the beginning of the deposition (Fig. S1a†). In this shaping process, BO_3^{3-} ions play roles

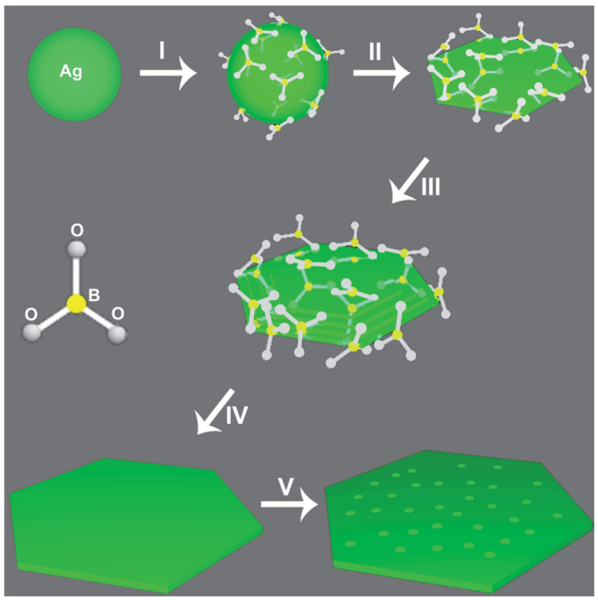

Fig. 3 Schematic illustration of the formation process of the highly surface-roughened Ag nanoplates. Process I: borate ions attached onto Ag nuclei. Process II: spherical Ag nuclei evolved into nanoplates under the protection of borate ions. Process III: slow layer-by-layer growth mode which increases the thickness. Process IV: formation of large Ag nanoplates. Process V: corrosive effects led to the formation of highly surface-roughened Ag nanoplates.

complementary to those of the conventional organic capping agents (*e.g.*, polyvinylpyrrolidone molecules that bind strongly to the {100} planes).[30] As electrodeposition proceeds for about 1 min, nanoparticles disappear and nanoplates with different sizes emerge. From the enlarged images, we can clear observe the layer-by-layer growth mode of the thickening process (Fig. S1b†). Due to the protection of BO_3^{3-} ions of {111} planes, the thickening growth is greatly supressed compared with the radial direction growth, leading to the formation of large while thin Ag nanoplates (Fig. S1e†). According to the growth mechanism summarized in Fig. 3, we anticipate that the concentration of BO_3^{3-} ions should aid in defining the deposited nanostructures.

To verify this expectation, we conducted experiments to investigate the effects of the concentration of H_3BO_3 in the electrolyte solution on the resulting Ag nanostructures. Our experimental results demonstrated that electrodeposition without H_3BO_3 in the electrolyte yielded only a nanoparticle film (Fig. 4a). Even with only a small amount of H_3BO_3 (*e.g.*, 0.16 M) in the electrolyte, nanoplates grew readily. Increasing the amount of H_3BO_3 from 0.16 M to 0.32 M produced sharp nanoplates with irregular shapes (Fig. 4b and c). The nanoplates deposited using higher concentrations of H_3BO_3 were also thinner than those deposited at lower H_3BO_3 concentrations, with thicknesses around 20 nm (Fig. 4d). These results verify that varying boric acid concentrations in the electrolyte during electrodeposition enables successful fabrication and allows for structural manipulation of the Ag nanoplates. Few studies have been devoted to the adsorption behavior of BO_3^{3-} ions on Ag

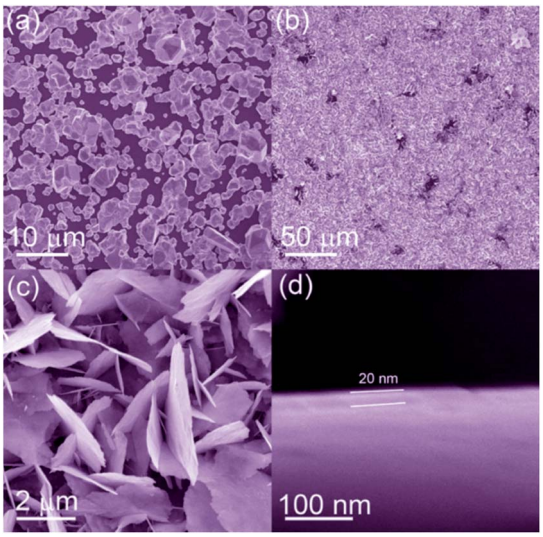

Fig. 4 The role of the H_3BO_3 concentration in the electrolyte. SEM images of the deposited Ag structures at different concentrations of (a) 0 M; (b–d) 0.32 M H_3BO_3 in the electrolyte solution. The deposition time is always 10 min.

nuclei. Our experiments illustrate that BO_3^{3-} ions are good candidates for stabilizing the {111} planes of Ag. BO_3^{3-} ions selectively inhibit the layer-by-layer growth process by which the nanoplates thicken, resulting in more lateral than vertical growth (with a corresponding ratio of about 100 : 1). Similarly, using BO_3^{3-} ions as shaping agents, Pt nanoplates were prepared (ESI, Fig. S3†), evidencing the robustness of BO_3^{3-} ions in controlling the shape of electroplated metallic nanostructures (Fig. 4).

2.3 Roughening process for the Ag nanoplates

SEM images clearly show that the nanoplate surfaces become more coarse later in the deposition process, but our current experimental results make it difficult to completely explain this roughening phenomenon. One likely possibility is that the OH^- ions were oxidized into O_2 around the anode (eqn (1)), thus the pH value decreased rapidly due to the consumption of OH^- ions.[33,34] Therefore, we believe that HNO_3, formed during the

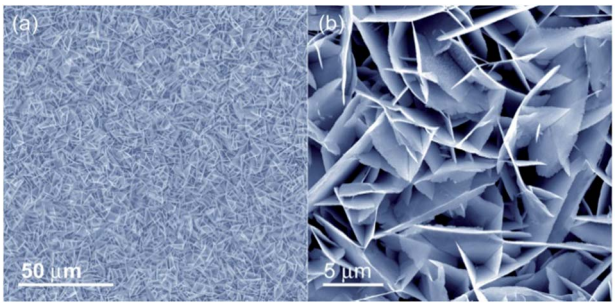

Fig. 5 (a and b) Ag nanoplates electroplated on a Si wafer covered by a thin-film (approximately 10 nm) layer of gold. The deposition time is 10 min.

deposition process, must be a key reactant in carving the smooth-surfaced Ag nanoplates into the more coarse ones.[35,36] This assumption is consolidated by the single crystalline nature of the coarse Ag nanoplates (Fig. 2).

$$\text{Anode: } 4OH^- - 2e \rightarrow O_2\,(g) \uparrow + 2H_2O$$

$$\text{Cathode: } Ag^+ + e \rightarrow Ag \quad (1)$$

In order to further test this hypothesis, HNO_3 aqueous solutions were used to treat smooth Ag nanoplates. As anticipated, coarse-surface Ag nanoplates, similar to those shown in Fig. 1, were obtained. Furthermore, $HPtCl_4$ aqueous solutions were used to achieve the same corrosive effect on the Ag nanoplates as HNO_3. Immersion in 0.05 M $HPtCl_4$ for 24 h transformed the smooth surfaces to coarse ones (ESI, Fig. S4†). During the corrosion process, the thickness of the nanoplates was reduced dramatically due to the fact that during the galvanic displacement reactions each Pt^{3+} ion consumed three Ag atoms. These results illustrated that Ag nanoplates could be transformed into nanoplates of other materials, such as Pt, Au, and Pd, expanding their potential application areas. Although post-synthesis etching treatments of nanoparticles have been used to create unique anisotropic nanostructures (*e.g.*, concave octahedrons and nanostars),[33] there are no reports on applying etching methods to *in situ* carve nanostructures during electrochemical growth. This is the first demonstration that corrosion induced by a change in the local pH value during electrochemical deposition can be used to carve the surface of electrodeposited nanostructures.

Based on our understanding of the Ag nanoplate formation mechanism, the nature of the cathode surface (*e.g.*, roughness) will be of prime importance in defining the initial nucleation sites during electrochemical deposition of Ag. For example, if a thin layer of Au film (*e.g.*, 10 nm) was thermally evaporated on the cathode surface prior to electrochemical deposition; the uniformity of the Ag nanoplate was significantly improved. As shown in Fig. 5, thin, extremely uniform Ag nanoplates with plate areas close to 10 μm were yielded on a very large scale. These Ag nanoplates grew into 3D forest-like nanoplate arrays. The 3D structure caused by nanoplate protrusion gives rise to an extremely high surface area-to-volume ratio,[37] as none of the faces of the nanoplates are completely obscured. The resulting nanoplates constituted a significant breakthrough; never before have Ag nanoplate arrays been reported to be produced on such a large scale and of such a high quality. Overall, results from varying the deposition parameters consolidate that the Ag nanoplate structures (*e.g.*, thickness, roughness, and size) can be tailored by modifying a combination of the electrolytic H_3BO_3 concentration, the deposition voltage, and the deposition time. More importantly, the Ag nanoplates with rough and clean surfaces free of the organic contamination that typically plagues Ag nanostructures formed using conventional anisotropic fabrication processes make them ideal for sensing applications.

2.4 SERS performance and biosensing applications

Their high purity and surface roughness allow these Ag nanoplate arrays to be used as excellent SERS substrates.[37,38] In addition, the laser light is efficiently used because none of the faces of the nanoplates are completely obscured. The 3D structure of the highly surface-roughened Ag nanoplate array results in less than 10% reflection (ESI, Fig. S5†). Specifically, we expect that Ag nanoplates with coarse surfaces can enhance SERS signals much more strongly than smooth substrate surfaces owing to the increased number of hot spots generated by nanoscale pits and cracks on the coarse surfaces. Experimental results verified this hypothesis. The Raman signal intensity of Rhodamine 6G molecules absorbed on the highly surface-roughened Ag nanoplates was more than two orders of magnitude higher than that of the smooth nanoplates (ESI, Fig. S6 and S7†). The SERS enhancement factor of the highly surface-roughened Ag nanoplates was estimated to be $>10^9$ using 4-aminothiophenol as a test molecule (ESI, Fig. S8†), which is much higher than most previously reported values.[14,17,33,39] As a comparision, SERS measurements were performed on the Ag nanoparticles prepared by a sodium citrate reduction method[40] with sizes ranging from 50 nm to 80 nm (ESI, Fig. S9†). The SERS signal of R6G molecules adsorbed on the highly surface roughened Ag nanoplates is more than 2000 times higher than that of the Ag nanoparticles under the same experimental conditions. Thin Ag nanoplates grown on a thin layer of Au showed stronger SERS enhancement than thicker ones (ESI, Fig. S6†). To demonstrate that only the thin Ag nanoplates were responsible for SERS signal enhancement, measurements were taken from a Au film thermally evaporated on a glass slide. This Au film exhibited no observable SERS signals when analysed at the same probe molecule concentrations. Also, no SERS signals were observed on a 20 nm-thick Ag membrane that was thermally evaporated on a glass slide.

To fundamentally understand the mechanisms behind this improved SERS performance, we performed finite-difference time-domain (FDTD) numerical simulations which modelled the electromagnetic field distributions on the Ag nanoplates.[41] FDTD simulation results consolidate that extremely strong electromagnetic fields are located across the roughened Ag nanoplate surfaces (ESI, Fig. S10†), which contribute to the extraordinarily strong SERS sensitivity.

As a proof-of-concept demonstration, we utilized the highly surface-roughened Ag nanoplates to detect DNA, proteins, and viruses. To avoid potential heating influence caused by laser exposure, the power of the laser was maintained at approximately 100 μW in all of the following biodetections. We first used the rough Ag nanoplates to detect DNA without any surface modifications or labelling processes. Fig. 6a shows a SERS spectrum from single-stranded DNA. The source of each of the Raman peaks can be attributed to either the backbone of the DNA, or the nucleotide bases of adenine (A), thymine (T), guanine (G), and cytosine (C).[42–48] After DNA hybridization, distinct changes appeared in the SERS spectrum. DNA hybridization caused the 1370 cm^{-1} peak, originating from the T, A, and G, to shift to 1390 cm^{-1}. In addition, two new peaks

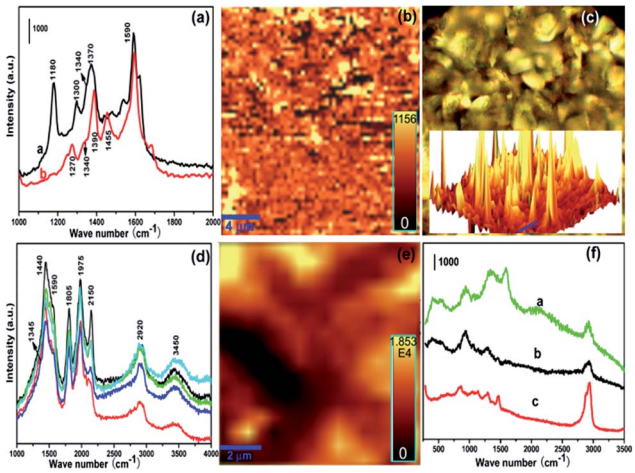

Fig. 6 (a) SERS spectra of single-stranded (curve a in black) and double-stranded DNA (curve b in red). (b) SERS mapping result for single-stranded DNA at 1590 cm^{-1}. (c) Optical image of the SERS substrate. Inset: 3D SERS mapping result corresponding to (b). (d) SERS spectra of Protein A/G at five randomly chosen sites. (e) SERS mapping result of Protein A/G at 1440 cm^{-1}. (f) SERS spectra of the rhinovirus type 4 (curve a in green), poliovirus type I wild-type (curve b in black), and poliovirus type I Sabin (curve c in red).

appeared at 1270 cm^{-1} and 1455 cm^{-1}. The 1270 cm^{-1} peak may have been caused by either the formation of new bonds or a change in bond orientation during the hybridization process. The 1455 cm^{-1} peak, originating from the out-of-plane vibrations of adenine rings, was likely created by both the rearrangement of adenine and the formation of an essentially flat adsorbate adenine ring on the SERS substrate.[44] These new peaks and peak shifts clearly prove that changes in the SERS spectrum can be used to detect DNA hybridization. A detailed analysis of the SERS-based DNA detection results can be found in the Experimental section in the ESI.† Fig. 6b and c display the good reproducibility of SERS signals resulting from the uniform distribution of hot spots on the rough Ag nanoplates. Fig. 6c exhibits an optical microscope image of the uniformly structured Ag nanoplate array.

Proteins are the machinery of life and participate in almost every cellular process.[49–52] Sensitive protein detection techniques allow researchers to gain a more thorough understanding of metabolic processes as well as to detect diseases in their early stages.[53] To demonstrate the benefits of using highly surface-roughened Ag nanoplate arrays in protein-specific SERS applications, we examined the Raman spectra of protein A/G. As shown in Fig. 6d, protein A/G exhibited strong Raman bands from the CH_2 (or CH_3) deformation mode at 1440 cm^{-1}, the guanine ring mode (at 1560 cm^{-1}), and the asymmetric stretching vibration of CH_2 (at 2920 cm^{-1}).[49–53] Five nanoplate sites chosen at random yielded nearly the same SERS spectra peaks, exhibiting intensity deviations below 10%. The excellent reproducibility of these SERS signals is mainly attributed to the uniform hot spot distribution on the Ag nanoplate arrays. The SERS mapping image of protein A/G (Fig. 6e) further proved the high SERS reproducibility from these Ag nanoplate arrays. Such SERS enhancements provided by these rough Ag nanoplates create new opportunities in protein detection. Most notably, in the future, coupling highly surface-roughened Ag nanoplates integrated with fast SERS detectors could provide an opportunity to monitor both protein kinetics and protein-receptor interactions.

We further applied our SERS substrate to the detection of three types of viruses: rhinovirus type 4, poliovirus type 1 Mahoney (PV1M), and poliovirus type 1 Sabin (PV1S). Fig. 6f shows the SERS spectra of the three viruses. In the SERS spectrum of rhinovirus (curve a in Fig. 6f), 400 cm^{-1}, 550 cm^{-1}, 935 cm^{-1}, 1370 cm^{-1}, 1585 cm^{-1}, and 2910 cm^{-1} peaks can be attributed to the symmetric out-of-plane bending mode of six-carbon rings, the disulfide stretching mode, the asymmetric bending mode of the five-carbon rings, the stretching vibration of C–N within adenine (or scissoring mode of CH_2), tryptophan, and the asymmetric stretching vibration of CH_2, respectively.[54]

As for the SERS spectra (curves b and c in Fig. 6f) for the two polioviruses, large peak-shifts between the PV1M and the PV1S indicate that these SERS substrates can be used to distinguish small structural changes. Specifically, the following specific peaks (and hence their associated molecular structure) were visible in PV1S: the 830 cm^{-1} (O–P–O symmetric stretch),[55] 1060 cm^{-1} (ribose, phenylalanine),[55] 1295 cm^{-1} (amide III from protein),[56] 1460 cm^{-1} (amide II, C–N stretching mode),[57] and 2940 cm^{-1} (the asymmetric stretching vibration of CH_2). In PV1M, the peaks shifted to 850 cm^{-1}, 1040 cm^{-1}, 1300 cm^{-1}, 1470 cm^{-1}, and 2945 cm^{-1}, respectively. The 940 cm^{-1} (C–C stretch in proteins)[55] peak disappeared in the PV1S SERS spectrum and was replaced by a new peak located at 645 cm^{-1} (an out-of-plane bending of carbon six-membered ring from adenine).[58] These results indicated that by using this new SERS substrate, it was possible to distinguish between small changes in the pathogen structure without complex chemical or biological treatments to either the virus sample or to the SERS substrate. The combination of simplicity, high sensitivity, and label-free identification makes our highly surface roughened Ag nanoplate arrays extremely attractive as a convenient, low-cost, and high-quality SERS substrate for biosensing, bioanalyses, and diagnostics.[58,59]

3. Conclusion

In summary, we synthesized large-area, high-purity, and most importantly, highly surface-roughened Ag nanoplate arrays using a simple electroplating/etching method with inorganic borate ions as a capping agent. Layer-by-layer nanoplate growth combined with electrocorrosion created a massive number of nanoscale steps and pits, which were uniformly distributed across the Ag nanoplates. These numerous hot spots and uniform, high-purity, 3D surface structures collectively made these Ag nanoplates ideal for SERS-based biosensing applications. To demonstrate the robustness of these nanoplates as a SERS substrate, we performed SERS detection on DNA, proteins, and viruses. The DNA analysis revealed obvious spectral differences between single-stranded and double-stranded DNA, establishing the usefulness of SERS for rapid detection of DNA

hybridization. The highly surface-roughened Ag nanoplates enabled sensitive characterization of proteins with excellent reproducibility. Finally, small structural differences between different strains of viruses strongly shifted the SERS peaks, indicating that SERS substrates enhanced with Ag nanoplates would allow researchers to differentiate between pathogens. In addition, the surface-roughened Ag nanoplates eliminated the need for additional treatments or amplification agents during the SERS biodetection process. These current efforts devoted to the structural optimization of highly surface-roughened Ag nanoplate arrays will facilitate efficient, low-cost, and label-free SERS biosensing, perhaps leading to practical platforms for clinical diagnosis.

Acknowledgements

We thank B. Kiraly, M. I. Lasley, R. C. Kogan, and B. D. Kryzer in The Pennsylvania State University for editing the manuscript. We gratefully acknowledge the financial support from the National Institutes of Health (Director's New Innovator Award, 1DP2OD007209-01), the National Science Foundation (NSF), the Penn State Center for Nanoscale Science (MRSEC) under grant DMR-0820404, and Huck Innovative & Transformational Seed (HITS) Fund. Components of this work were conducted at the Penn State node of the NSF-funded National Nanotechnology Infrastructure Network.

Notes and references

1 X. M. Qian and S. M. Nie, *Chem. Soc. Rev.*, 2008, **37**, 912–920.
2 Y. B. Zheng, J. L. Payton, T. B. Song, B. K. Pathem, Y. X. Zhao, H. Ma, Y. Yang, L. Jensen, A. K. Y. Jen and P. S. Weiss, *Nano Lett.*, 2012, **12**, 5362–5368.
3 R. A. Alvarez-Puebla and L. M. Liz-Marzan, *Chem. Soc. Rev.*, 2012, **41**, 43–51.
4 R. A. Alvarez-Puebla, A. Agarwal, P. Manna, B. P. Khanal, P. Aldeanueva-Potel, E. Carbo-Argibay, N. Pazos-Perez, L. Vigderman, E. R. Zubarev, N. A. Kotov and L. M. Liz-Marzan, *Proc. Natl. Acad. Sci.*, 2011, **108**, 8157–8161.
5 Y. B. Zheng, J. L. Payton, C. H. Liu, R. Chung, S. Cheunkar, B. K. Pathem, Y. Yang, L. Jensen and P. S. Weiss, *Nano Lett.*, 2011, **11**, 3447–3452.
6 F. J. Garcia-Vidal and J. B. Pendry, *Phys. Rev. Lett.*, 1996, **77**, 1163–1166.
7 N. J. Halas, S. Lal, W.-S. Chang, S. Link and P. Nordlander, *Chem. Rev.*, 2011, **111**, 3913–3961.
8 R. A. Alvarez-Puebla, E. R. Zubarev, N. A. Kotov and L. M. Liz-Marzan, *Nano Today*, 2012, **7**, 6–9.
9 W. Li, P. H. C. Camargo, X. Lu and Y. Xia, *Nano Lett.*, 2008, **9**, 485–490.
10 S. K. Yang, W. P. Cai, L. C. Kong and Y. Lei, *Adv. Funct. Mater.*, 2010, **20**, 2527–2533.
11 S. Hong, T. Kang, D. Choi, Y. Choi and L. P. Lee, *ACS Nano*, 2012, **6**, 5803–5808.
12 C. Escobedo, A. G. Brolo, R. Gordon and D. Sinton, *Nano Lett.*, 2012, **12**, 1592–1596.
13 S. K. Yang, F. Xu, S. Ostendorp, G. Wilde, H. Zhao and Y. Lei, *Adv. Funct. Mater.*, 2011, **21**, 2446–2455.
14 Y. Wang, H. Wei, B. Li, W. Ren, S. Guo, S. Dong and E. Wang, *Chem. Commun.*, 2007, **48**, 5220–5222.
15 Y. Lu, G. L. Liu and L. P. Lee, *Nano Lett.*, 2005, **5**, 5–9.
16 Y. Lu, G. L. Liu, J. Kim, Y. X. Mejia and L. P. Lee, *Nano Lett.*, 2005, **5**, 119–124.
17 R. J. Newhouse, H. Wang, J. K. Hensel, D. A. Wheeler, S. Zou and J. Z. Zhang, *J. Phys. Chem. Lett.*, 2011, **2**, 228–235.
18 B. M. Ross, L. Y. Wu and L. P. Lee, *Nano Lett.*, 2011, **11**, 2590–2595.
19 S. Preciado-Flores, D. A. Wheeler, T. M. Tran, Z. Tanaka, C. Y. Jiang, M. Barboza-Flores, F. Qian, Y. Li, B. Chen and J. Z. Zhang, *Chem. Commun.*, 2011, **47**, 4129–4131.
20 H. Im, K. C. Bantz, N. C. Lindquist, C. L. Haynes and S. -H. Oh, *Nano Lett.*, 2010, **10**, 2231–2236.
21 Y. Yang, S. Matsubara, L. Xiong, T. Hayakawa and M. Nogami, *J. Phys. Chem. C*, 2007, **111**, 9095–9104.
22 S. Viarbitskaya, A. Teulle, R. Marty, J. Sharma, C. Girard, A. Arbouet and E. Dujardin, *Nat. Mater.*, 2013, **12**, 426–432.
23 X. Xia, J. Zeng, Q. Zhang, C. H. Moran and Y. Xia, *J. Phys. Chem. C*, 2012, **116**, 21647–21656.
24 I. Pastoriza-Santos and L. M. Liz-Marzan, *J. Mater. Chem.*, 2008, **18**, 1724–1737.
25 S. Guo, W. Liang and E. Wang, *Chem. Commun.*, 2007, **30**, 3163–3165.
26 X. Zhang, A. Hu, T. Zhang, W. Lei, X. Xue, Y. Zhou and W. W. Duley, *ACS Nano*, 2011, **5**, 9082–9092.
27 G. Liu, W. Cai, L. Kong, G. Duan and F. Lv, *J. Mater. Chem.*, 2010, **20**, 767–772.
28 B. Seo, S. Choi and J. Kim, *ACS Appl. Mater. Interfaces*, 2011, **3**, 441–446.
29 S. Murugesan, A. Akkineni, B. P. Chou, M. S. Glaz, D. A. V. Bout and K. J. Stevenson, *ACS Nano*, 2013, **7**, 8199–8205.
30 The mean size of the cavities on the surface-roughened Ag nanoplates was about 35 nm. The cavities were closely packed on both sides of the Ag nanoplates. Thus, we estimated the density of the cavities to be about 1.6×10^3 μm^{-2}. Since hot spots were mainly localized around the cavities (see simulation result shown in Fig. S9, ESI†), the hot spot density was estimated to be $>10^3$ μm^{-2}. Smooth Ag nanoplates were used as SERS substrates in most of the previous studies, where only a small number of hot spots were located around the sharp edges and corners (for example, see ref. 22) and contributed to the SERS enhancement. As a result, this work has one of the highest hot-spot densities achieved with Ag nanoplates.
31 D. Erickson, D. Sinton and D. Psaltis, *Nat. Photonics*, 2011, **5**, 583–590.
32 Our electrodeposited Ag nanoplates were cross-linked together and slanted relative to the substrate. Since no template was used, their formation sites and orientations were random. This random growth gives the Ag nanoplates an equal probability to grow at different sites across the substrates in different orientations. Therefore, the electrodeposited structure on the electrode has a uniformly

random morphology. This uniformity is much better than the nanoplate structures synthesized by chemical seed-mediated growth method (see S. R. Beeram and F. P. Zamborini, *ACS Nano*, 2010, **4**, 3633–3646) or the self-assembly approach (see X. Zhang, A. Hu, T. Zhang, W. Lei, X. Xue, Y. Zhou and W. W. Duley, *ACS Nano*, 2011, **5**, 9082–9092).

33 K. C. Leonard and A. J. Bard, *J. Am. Chem. Soc.*, 2013, **135**, 15890–15896.
34 A. J. Bard and R. W. Murray, *Proc. Natl. Acad. Sci. U. S. A.*, 2012, **109**, 11484.
35 M. J. Mulvihill, X. Y. Ling, J. Henzie and P. Yang, *J. Am. Chem. Soc.*, 2010, **132**, 268–274.
36 C. M. Cobley, M. Rycenga, F. Zhou, Z. Y. Li and Y. Xia, *Angew. Chem., Int. Ed.*, 2009, **48**, 4824–4827.
37 Y. Sun and C. Lei, *Angew. Chem., Int. Ed.*, 2009, **48**, 6824–6827.
38 Y. Sun, *Adv. Funct. Mater.*, 2010, **20**, 3646–3657.
39 L. Yang, B. Yan, W. R. Premasiri, L. D. Ziegler, L. Dal Negro and B. M. Reinhard, *Adv. Funct. Mater.*, 2010, **20**, 2619–2628.
40 S. Yang, W. Cai, G. Liu and H. Zeng, *J. Phys. Chem. C*, 2011, **113**, 7692–7696.
41 Y. Zhao, S. C. S. Lin, A. A. Nawaz, B. Kiraly, Q. Hao, Y. Liu and T. J. Huang, *Opt. Express*, 2010, **18**, 23458–23465.
42 S. A. Kazane, D. Sok, E. H. Cho, M. L. Uson, P. Kuhn, P. G. Schultz and V. V. Smider, *Proc. Natl. Acad. Sci.*, 2012, **109**, 3731–3736.
43 J. S. Suh and M. Moskovits, *J. Am. Chem. Soc.*, 1986, **108**, 4711–4718.
44 E. Papadopoulou and S. E. J. Bell, *Angew. Chem., Int. Ed.*, 2011, **50**, 9058–9061.
45 G. Zheng, L. Qin and C. A. Mirkin, *Angew. Chem., Int. Ed*, 2008, **47**, 1938–1941.
46 A. Barhoumi and N. J. Halas, *J. Am. Chem. Soc.*, 2010, **132**, 12792–12793.
47 A. Barhoumi, D. Zhang and N. J. Halas, *J. Am. Chem. Soc.*, 2008, **130**, 14040–14041.
48 X. X. Han, B. Zhao and Y. Ozaki, *Anal. Bioanal. Chem.*, 2009, **394**, 1719–1727.
49 X. Han, Y. Wang, Z. Lu, C. Wang, W. Xu, B. Zhao and Y. Ozaki, *Anal. Chem.*, 2008, **80**, 2799–2804.
50 X. X. Han, G. G. Huang, B. Zhao and Y. Ozaki, *Anal. Chem.*, 2009, **81**, 3329–3333.
51 X. Yang, C. Gu, F. Qian, Y. Li and J. Z. Zhang, *Anal. Chem.*, 2011, **83**, 5888–5894.
52 R. Tuma, *J. Raman Spectrosc.*, 2005, **36**, 307–319.
53 S. Shanmukh, L. Jones, J. Driskell, Y. Zhao, R. Dluhy and R. A. Tripp, *Nano Lett.*, 2006, **6**, 2630–2636.
54 T. A. Turano and K. A. Hartman, *J. Phys. Chem.*, 1976, **80**, 1157–1163.
55 W. T. Cheng, M. T. Liu, H. N. Liu and S. Y. Lin, *Microsc. Res. Tech.*, 2005, **68**, 75–79.
56 Z. Movasaghi, S. Rehman and I. U. Rehman, *Appl. Spectrosc. Rev.*, 2007, **42**, 493–541.
57 K. Malek, E. Podstawka, J. Milecki, G. Schroeder and L. M. Proniewicz, *Biophys. Chem.*, 2009, **142**, 17–26.
58 K. M. Mayer and J. H. Hafner, *Chem. Rev.*, 2011, **111**, 3828–3857.
59 M. Yang, R. Alvarez-Puebla, H. S. Kim, P. Aldeanueva-Potel, L. M. Liz-Marzan and N. A. Kotov, *Nano Lett.*, 2010, **10**, 4013–4019.